

# Rôle of kinetic transport coefficients for hydrodynamic simulations of granular flow

Lidia Almazán,<sup>1</sup> José A. Carrillo,<sup>2</sup> Clara Salueña,<sup>3</sup> Vicente Garzó,<sup>4</sup> and Thorsten Pöschel<sup>1</sup>

<sup>1</sup>*Institute for Multiscale Simulation, Universität Erlangen-Nürnberg, D-91052 Erlangen, Germany*

<sup>2</sup>*Institució Catalana de Recerca i Estudis Avançats and Departament de Matemàtiques, Universitat Autònoma de Barcelona, E-08193 Bellaterra, Spain*

<sup>3</sup>*Departament d'Enginyeria Mecànica, Universitat Rovira i Virgili, 43007 Tarragona, Spain*

<sup>4</sup>*Departamento de Física, Universidad de Extremadura, E-06071 Badajoz, Spain*

(Dated: April 11, 2012)

A numerical study is presented to assess the performance of two different models of kinetic transport coefficients for granular materials, namely the Jenkins-Richman theory for moderately dense, quasielastic grains, and the improved Lutsko-Garzó theory for arbitrary inelasticity. For this purpose a time-dependent problem such as the granular Faraday instability is selected to perform numerical simulations of the granular Navier-Stokes equations. Both solutions are compared with event-driven simulations of the same system under the same conditions, by analyzing the density, the temperature and the velocity field. Important differences are found between the two models leading to interesting implications. In particular the heat transfer mechanism coupled to the density gradient which is a distinctive feature of inelastic granular gases, is responsible for a major discrepancy in the temperature field and hence in the diffusion mechanisms.

## I. INTRODUCTION

The hydrodynamics of granular materials is far from being well understood. The first difficulty comes from the kinetic theory level, where the far-from-equilibrium nature of the problem leads to both conceptual and technical limitations. Many contributions, starting in the '80 of the last century [1, 2], have helped to develop a well established hydrodynamic theory of granular gases, including mixtures and multi-component materials. However the application to other types of granular materials is still uncertain.

In academy as well as in industry, one would like to have a good numerical solver for a variety of granular flow problems under different conditions. In the process of going from theory to real applications, one must resort to good choices of kinetic transport coefficients to ensure the appropriate modeling of the system. Strictly speaking, kinetic theory expansions cease to be valid as we enter the realm of moderately dense gases. On the other hand, a purely empirical approach, like the one used for regular liquids and where one measures the transport coefficients, to use them later in the Navier-Stokes equations, does not apply for granular hydrodynamics. The reason is that the system properties depend on a tricky combination of the ingredients, each one of them inextricably linked to the rest. The inherent difficulty of these problems lies on the dissipative character of real grain interactions, which is responsible for microscopic irreversibility, lack of scale separation, mesoscopic nature of the flow, and strong nonlinearities in the governing equations.

Numerical validation of transport coefficients from kinetic theories has been analyzed for the Jenkins-Richman expressions [1, 2] by molecular dynamics simulations in [3] and in experiments such as granular flow past an obstacle [4] and vertically oscillated granular layers [5–9]. This choice as a test case for hydrodynamic theories comes from being one of the simplest experiments

in which all different regimes of the granular flow are present while leading to interesting standing-wave pattern formation and dynamics [10, 11], clustering [12, 13] and phase transitions [14–16].

In a previous paper [7] we studied computationally the Faraday instability [17] in vibrated granular disks, comparing the output from hydrodynamic and particle simulations in detail. This served to validate a Navier-Stokes code for granular material based on a WENO (Weighted Essentially Non-Oscillatory) approach [18] which is capable of capturing the features of the highly supersonic flow generated by the impact of a piston. For this purpose we used the well-known Jenkins-Richman expressions [1, 2] for the kinetic coefficients, valid for moderately dense gases in the limit of vanishing inelasticity. The conclusion of the study was that, even far beyond the conditions where the kinetic theory expansions are valid, the results showed qualitative and quantitative agreement with those from event-driven molecular dynamics simulations, in a range of parameters which covered the entire bifurcation diagram of the Faraday instability at the coefficient of restitution  $\alpha = 0.75$ . The errors did not exceed 20%.

The Jenkins-Richman (JR) theory, however, fails describing the heat flux accurately, since in the limit of elastic gases the heat flux term coupled to the density gradient vanishes. Beyond the JR theory, more recently kinetic expansions at finite inelasticity have been developed to model moderately dense gases [19–21]. Here we follow a similar approach to [7], that is, we will use the kinetic transport coefficients derived in [19–21] to compare the performance of the granular Navier-Stokes solver with respect to particle simulations. We will also analyze the differences between the results provided by the JR theory and those from the current theory, to check whether the use of proper kinetic transport coefficients reduces the aforementioned discrepancy.

## II. HYDRODYNAMIC THEORY OF GRANULAR GASES

We consider a granular fluid composed of smooth inelastic hard disks of unit mass  $m = 1$  and diameter  $\sigma$ . Collisions are characterized by a (constant) coefficient of normal restitution  $0 < \alpha \leq 1$ . In a kinetic theory description, the relevant information on the system is contained in the one-particle velocity distribution function. At *moderate* densities and assuming molecular chaos, the velocity distribution function obeys the (inelastic) Enskog kinetic equation [22, 23]. Starting from this kinetic theory, one can easily obtain the (macroscopic) hydrodynamic equations for the number density  $n(\vec{r}, t)$ , the flow velocity  $\vec{u}(\vec{r}, t)$ , and the local temperature  $T(\vec{r}, t)$  [24]. In the case of two-dimensional granular gases, the balance equations read

$$\frac{\partial n}{\partial t} + \vec{\nabla} \cdot (n\vec{u}) = 0, \quad (1)$$

$$n \left( \frac{\partial \vec{u}}{\partial t} + \vec{u} \cdot \vec{\nabla} \vec{u} \right) = -\vec{\nabla} \cdot \hat{P} + n\vec{F}, \quad (2)$$

and

$$n \left( \frac{\partial T}{\partial t} + \vec{u} \cdot \vec{\nabla} T \right) = -\nabla \cdot \vec{q} - \hat{P} : \vec{\nabla} \vec{u} - \zeta n T. \quad (3)$$

In the above equations,  $\vec{F}$  is the external force per unit mass acting on the system,  $\hat{P}$  is the pressure tensor,  $\vec{q}$  is the heat flux, and  $\zeta$  is the cooling rate due to the energy dissipated in collisions. It is worthwhile to note that the macroscopic equations given in Eqs. (1)-(3) differ from their counterparts for elastic fluids only via the appearance of the cooling rate  $\zeta$  on the right-hand side of Eq. (3). On the other hand, the corresponding transport coefficients defining the momentum and heat fluxes must depend in general on the coefficient of restitution  $\alpha$ .

As it happens for elastic fluids, the usefulness of the balance equations (1)-(3) is limited unless the fluxes and the cooling rate are specified in terms of the hydrodynamic fields and their spatial gradients. To first order in the spatial gradients, the Navier-Stokes constitutive equations provide a link between the exact balance equations and a closed set of equations for the hydrodynamic fields. The constitutive relation of the pressure tensor  $P_{ij}$  is

$$P_{ij} = p\delta_{ij} - \eta \left( \partial_j u_i + \partial_i u_j - \delta_{ij} \vec{\nabla} \cdot \vec{u} \right) - \gamma \delta_{ij} \vec{\nabla} \cdot \vec{u}, \quad (4)$$

where  $p$  is the hydrostatic pressure,  $\eta$  is the shear viscosity, and  $\gamma$  is the bulk viscosity. The constitutive equation for the heat flux is

$$\vec{q} = -\kappa \vec{\nabla} T - \mu \vec{\nabla} n, \quad (5)$$

where  $\kappa$  is the coefficient of thermal conductivity, and  $\mu$  is a new coefficient which does not have an analogue for a

gas of elastic particles. Finally, to first order in gradients, the cooling rate  $\zeta$  can be written as [22]

$$\zeta = \zeta_0 + \zeta_1 \nabla \cdot \vec{u}. \quad (6)$$

The explicit forms of the hydrostatic pressure  $p$ , the Navier-Stokes transport coefficients  $\eta$ ,  $\gamma$ ,  $\kappa$ , and  $\mu$  and the coefficients  $\zeta_0$  and  $\zeta_1$  can be obtained by solving the corresponding Enskog equation. However, due to the mathematical complexity of this kinetic equation, only approximate results for the above coefficients can be obtained. Here, we consider two independent approaches for hard disks proposed by Jenkins and Richman [2] and Lutsko and Garzó [19, 21]. Let us consider each method separately.

### A. Jenkins-Richman (JR) theory

The results derived by Jenkins and Richman [1, 2] are obtained by solving the Enskog equation for spheres [1] and disks [2] by means of Grad's method [25]. The idea behind Grad's moment method is to expand the velocity distribution function in a complete set of orthogonal polynomials (generalized Hermite polynomials), the coefficients being the corresponding velocity moments. Next, the expansion is truncated after a certain order  $k$ . When this truncated expansion is substituted into the hierarchy of moment equations up to order  $k$  one gets a closed set of coupled equations. In the case of a two-dimensional system, the eight retained moments are the hydrodynamic fields ( $n$ ,  $\vec{u}$ , and  $T$ ) plus the irreversible momentum and heat fluxes ( $P_{ij} - p\delta_{ij}$  and  $\vec{q}$ ).

Although the application of Grad's method to the Enskog equation is not restricted to nearly elastic particles, the results derived by Jenkins and Richman [2] (JR theory) neglect the cooling effects on temperature due to the cooling rate in the expressions of the transport coefficients [see for instance, Eqs. (70), (89), (98), (99), and (100) of Ref. [2] when the disks are smooth]. Given that this assumption can only be considered as acceptable for nearly elastic systems, the authors of Ref. [2] conclude that their theory only holds in the quasielastic limit ( $\alpha \rightarrow 1$ ).

The explicit forms of the hydrostatic pressure, the Navier-Stokes transport coefficients and the cooling rate in the JR theory are given by

$$p_{\text{JR}} = \frac{4}{\pi\sigma^2} \phi T [1 + (1 + \alpha)G(\phi)], \quad (7)$$

$$\eta_{\text{JR}} = \frac{\phi}{2\sigma} \sqrt{\frac{T}{\pi}} \left[ \frac{1}{G(\phi)} + 2 + \left(1 + \frac{8}{\pi}\right) G(\phi) \right], \quad (8)$$

$$\gamma_{\text{JR}} = \frac{8}{\pi\sigma} \phi G(\phi) \sqrt{\frac{T}{\pi}}, \quad (9)$$

$$\kappa_{\text{JR}} = \frac{2\phi}{\sigma} \sqrt{\frac{T}{\pi}} \left[ \frac{1}{G(\phi)} + 3 + \left( \frac{9}{4} + \frac{4}{\pi} \right) G(\phi) \right], \quad (10)$$

$$\mu_{\text{JR}} = 0,$$

$$\zeta_{0,\text{JR}} = \frac{4}{\sigma} (1 - \alpha^2) \sqrt{\frac{T}{\pi}} G(\phi), \quad (11)$$

$$\zeta_{1,\text{JR}} = 0.$$

In the above equations,  $\phi = n\pi\sigma^2/4$  is the (dimensionless) volume fraction occupied by the granular disks, also called packing fraction,  $G(\phi) = \phi\chi(\phi)$ , and  $\chi(\phi)$  is the pair correlation function.

Because of the assumption of near elastic particles in the JR theory, Eqs. (7)–(11) show clearly that the coefficient of restitution  $\alpha$  only enters in the equation of state (7) and in the expression (11) for the zeroth-order cooling rate  $\zeta_0$ . At this level of approximation, the expressions of the Navier-Stokes transport coefficients  $\eta_{\text{JR}}$ ,  $\gamma_{\text{JR}}$ , and  $\kappa_{\text{JR}}$  are the same as those given by the Enskog equation for elastic disks [26].

In order to get the dependence of the transport coefficients and the cooling rate in both JR and LG theories, one has to choose an approximate form for the pair correlation function  $\chi(\phi)$ . In this paper, we have chosen the forms proposed by Torquato [27],

$$\chi(\phi) = \begin{cases} \frac{1 - \frac{7}{16}\phi}{(1 - \phi)^2} & \text{for } 0 \leq \phi < \phi_f, \\ \frac{1 - \frac{7}{16}\phi_f}{(1 - \phi_f)^2} \frac{\phi_c - \phi}{\phi_c - \phi_f} & \text{for } \phi_f \leq \phi \leq \phi_c, \end{cases} \quad (12)$$

which go through the freezing point  $\phi_f = 0.69$  and approach the random close packing fraction,  $\phi_c = 0.82$  with reasonable accuracy.

## B. Lutsko-Garzó (LG) theory

The results derived independently by Lutsko [19] and Garzó [21] (LG theory) are based on the application of the Chapman-Enskog expansion [28] to the Enskog equation. Both works extend previous results [20] obtained for hard spheres to an arbitrary number of dimensions. The Chapman-Enskog method is a procedure to construct an

approximate perturbative solution to the Enskog equation in powers of the spatial gradients. More specifically, one assumes that the spatial variations of the hydrodynamic fields  $n$ ,  $\vec{u}$ , and  $T$  are small on the scale of the mean free path. On the other hand, while the strength of the gradients can be controlled by the boundary conditions in the case of elastic collisions, the problem is more complicated for granular fluids since in some cases (e.g., steady states such as the simple shear flow [29, 30]) there is an intrinsic relation between dissipation and some hydrodynamic gradient. The LG theory considers situations where the spatial gradients are sufficiently small and *independent* of the coefficient of restitution  $\alpha$ . As a consequence, the corresponding forms of the Navier-Stokes transport coefficients are not limited *a priori* to weak inelasticity since they incorporate the complete nonlinear dependence on  $\alpha$ .

As for elastic collisions [28], the transport coefficients in the Chapman-Enskog method are given in terms of the solutions of a set of coupled linear integral equations that are solved by means of a polynomial Sonine expansion. For simplicity, usually only the lowest Sonine polynomial (first Sonine approximation) is retained [19, 20] and the results obtained from this simple approach agree well with Monte Carlo simulations, except for the heat flux transport coefficients at high dissipation [31, 32]. Motivated by this disagreement, a modified version of the first Sonine approximation has been proposed [33]. The modified Sonine approximation replaces the Gaussian weight function (used in the standard Sonine method) by the homogeneous cooling state distribution. This new method significantly improves the  $\alpha$ -dependence of  $\kappa$  and  $\mu$  since partially eliminates the discrepancies between simulation and theory for quite strong dissipation (see for instance, Figs. 1-3 of Ref. [33]). The modified Sonine solution has been recently employed by Garzó [21] to determine the Navier-Stokes transport coefficients of dense  $d$ -dimensional granular gases.

The results obtained in the LG theory for the equation of state and the Navier-Stokes transport coefficients for hard disks ( $d = 2$ ) are

$$p_{\text{LG}} = p_{\text{JR}} = \frac{4}{\pi\sigma^2} \phi T [1 + (1 + \alpha)G(\phi)], \quad (13)$$

$$\gamma_{\text{LG}} = \frac{4}{\pi\sigma} \phi G(\phi) \sqrt{\frac{T}{\pi}} (1 + \alpha) \left( 1 - \frac{c}{32} \right), \quad (14)$$

$$\eta_{\text{LG}} = \frac{\sqrt{T/\pi}}{2\sigma} \frac{[1 - \frac{1}{4}(1 + \alpha)(1 - 3\alpha)G(\phi)] [1 + \frac{1}{2}G(\phi)(1 + \alpha)]}{\nu_\eta^* - \frac{1}{2}\zeta_0^*} + \frac{1}{2}\gamma_{\text{LG}}, \quad (15)$$

$$\kappa_{\text{LG}} = \frac{2}{\sigma} \sqrt{\frac{T}{\pi}} \left\{ \left[ 1 + \frac{3}{4}G(\phi)(1 + \alpha) \right] \kappa_k^* + \frac{2}{\pi} \phi G(\phi)(1 + \alpha) \left( 1 + \frac{7c}{32} \right) \right\}, \quad (16)$$

$$\mu_{\text{LG}} = \frac{T\sigma}{\phi} \sqrt{\pi T} \left[ 1 + \frac{3}{4} G(\phi)(1 + \alpha) \right] \mu_k^* \quad (17)$$

where the (reduced) kinetic contributions  $\kappa_k^*$  and  $\mu_k^*$  are

$$\kappa_k^* = \frac{1 + c + \frac{3}{8} G(\phi)(1 + \alpha)^2 [2\alpha - 1 + \frac{c}{2}(1 + \alpha)]}{2(\nu_\kappa^* - 2\zeta_0^*)}, \quad (18)$$

$$\mu_k^* = \frac{\zeta_0^* \kappa_k^* (1 + \phi \partial_\phi \ln \chi) + \frac{c}{4} + \frac{3}{8} G(\phi)(1 + \alpha) (1 + \frac{1}{2} \phi \partial_\phi \ln \chi) [\alpha(\alpha - 1) + \frac{c}{12} (14 - 3\alpha + 3\alpha^2)]}{2\nu_\kappa^* - 3\zeta_0^*}. \quad (19)$$

In Eqs. (15)–(19) we have introduced the quantities [21]

$$\zeta_0^* = \frac{1}{2} \chi(\phi)(1 - \alpha^2) \left( 1 + \frac{3c}{32} \right), \quad (20)$$

$$\nu_\eta^* = \frac{1}{8} \chi(\phi)(7 - 3\alpha)(1 + \alpha) \left( 1 + \frac{7c}{32} \right), \quad (21)$$

$$\nu_\kappa^* = \frac{1}{4} \chi(\phi)(1 + \alpha) \left[ 1 + \frac{15}{4} (1 - \alpha) + \frac{365 - 273\alpha}{128} c \right], \quad (22)$$

where

$$c(\alpha) = \frac{32(1 - \alpha)(1 - 2\alpha^2)}{57 - 25\alpha + 30\alpha^2(1 - \alpha)} \quad (23)$$

is the fourth cumulant coefficient measuring the deviation of the homogeneous reference state from its Gaussian form. Also taking into account Eq. (12), we obtain the expression

$$\frac{\partial}{\partial \phi} \ln \chi(\phi) = \begin{cases} \frac{25 - 7\phi}{(16 - 7\phi)(1 - \phi)} & \text{for } 0 \leq \phi < \phi_f \\ \frac{1}{(\phi_c - \phi)} & \text{for } \phi_f \leq \phi < \phi_c \end{cases}, \quad (24)$$

to be used in Eq. (19).

It is quite apparent that, except the equation of state (13), the expressions for the Navier-Stokes transport coefficients of the LG theory clearly differ from those obtained in the JR theory. In fact, Eqs. (14), (15), (16), and (17) of the LG theory reduce to Eqs. (8), (9), and (10), respectively, in the elastic limit ( $\alpha = 1$ , and so  $\zeta_0^* = c = 0$ ). Note that the expressions derived by Lutsko [19] neglect in the expressions (21) and (22) of  $\nu_\eta^*$  and  $\nu_\kappa^*$ , respectively, the factors of  $c$  coming from the non-Gaussian corrections to the reference state. These extra factors will be accounted for in our numerical results since their effect on transport becomes non negligible at small values of  $\alpha$ . In Fig. 1 we show the ratio between the bulk viscosity, shear viscosity, and thermal conductivity given by the LG and JR theories as a function of the coefficient of restitution for different packing fractions. Note that the bulk viscosity ratio does not depend on  $\phi$ . We also observe the order of magnitude of the new term in

the heat flux due to the density gradient in the LG theory with respect to the heat flux of the JR theory. The quantitative percentage of deviation of the transport coefficients with the LG theory from the JR theory is quite significant for  $\alpha = 0.8$  and the different packing fractions  $\phi$  used. We emphasize how the LG-term related to the density gradient in the heat flux becomes very important for  $\alpha \leq 0.8$ .

Finally, the contributions to the cooling rate are given by

$$\zeta_{0,\text{LG}} = \frac{4}{\sigma} (1 - \alpha^2) \sqrt{\frac{T}{\pi}} G(\phi) \left( 1 + \frac{3c}{32} \right), \quad (25)$$

$$\zeta_{1,\text{LG}} = \frac{3}{2} G(\phi)(1 - \alpha^2) \left[ \frac{3}{32} \frac{\frac{1}{8} \omega^* - c(1 + \alpha)(\frac{1}{3} - \alpha)}{\nu_\kappa^* - \frac{3}{4}(1 - \alpha^2)} - 1 \right], \quad (26)$$

where

$$\nu_\zeta^* = -\frac{1 + \alpha}{192} (30\alpha^3 - 30\alpha^2 + 153\alpha - 185), \quad (27)$$

$$\omega^* = (1 + \alpha) \left[ (1 - \alpha^2)(5\alpha - 1) - \frac{c}{12} (15\alpha^3 - 3\alpha^2 + 69\alpha - 41) \right]. \quad (28)$$

Equation (25) agrees with its corresponding counterpart in the JR theory, Eq. (11), when one neglects the non-Gaussian corrections to the reference state ( $c = 0$ ). Note that  $\zeta_1$  vanishes in limits of elastic gases ( $\alpha = 1$ , arbitrary volume fraction  $\phi$ ) and of dilute inelastic gases ( $\phi = 0$ , arbitrary values of the coefficient of restitution  $\alpha$ ). In Fig. 2, we plot the  $\alpha$ -dependence of  $\zeta_{1,\text{LG}}$ . We observe that the first-order contribution to the total cooling rate appears to be more significant as the gas becomes denser.

### C. Numerical scheme for the hydrodynamic granular equations

The compressible Navier-Stokes-like equations for granular materials (1), (2), and (3) are solved in conservation form for the convective terms, that is, we numerically solve the system for the density, the momentum

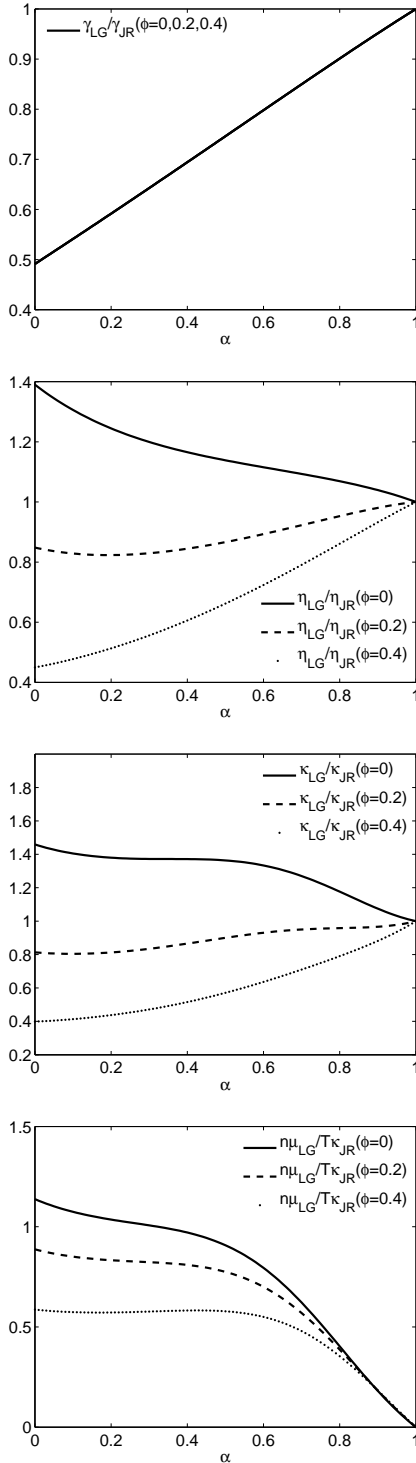


FIG. 1: Bulk viscosity ratio  $\gamma_{LG}/\gamma_{JR}$  (top), shear viscosity ratio  $\eta_{LG}/\eta_{JR}$  (second), thermal conductivity ratio  $\kappa_{LG}/\kappa_{JR}$  (third), and  $n\mu_{LG}/T\kappa_{JR}$  ratio (bottom) as a function of the restitution coefficient  $\alpha$  for three different values of the packing fraction  $\phi$ :  $\phi = 0$  (solid line),  $\phi = 0.2$  (dashed line), and  $\phi = 0.4$  (dotted line).

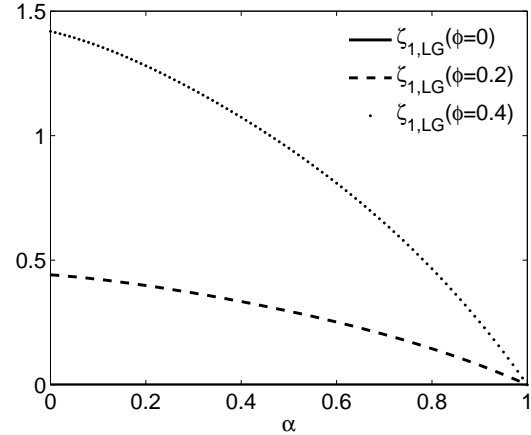


FIG. 2: First order correction of the cooling coefficient for LG theory as a function of the coefficient of restitution  $\alpha$  for three different values of the packing fraction  $\phi$ :  $\phi = 0$  (solid line),  $\phi = 0.2$  (dashed line), and  $\phi = 0.4$  (dotted line).

and the total energy:  $(n, n\vec{u}, W)$  where the total energy density  $W$  is given by

$$W = nT + \frac{1}{2}n|\vec{u}|^2. \quad (29)$$

This system can be rewritten as a system of nonlinear conservation laws with sources as in Ref. [7]. Local eigenvalues and both local left- and right-eigenvectors of the Jacobian matrices of the fluxes are explicitly computable (see Appendix of Ref. [7]). We only mention here that the characteristic speeds of the waves in the hyperbolic part of the equation can be written in terms of the speed of sound, given by

$$c_s^2 = \frac{\partial p}{\partial n} + \frac{p}{n^2} \frac{\partial p}{\partial \epsilon}, \quad (30)$$

for a general equation of state where  $p = p(n, \epsilon)$  with the enthalpy  $\epsilon = T$  for a two dimensional system. We refer to Ref. [7] for the full details of the numerical scheme that here is applied to both the LG and the JR hydrodynamic equations since they share the same structure. Let us just briefly mention that Navier-Stokes terms are treated by simple centered high-order explicit in time finite difference approximations and considered as sources for the method of lines in the time approximation. Meanwhile the Euler (convective) terms are solved in local coordinates by a fifth-order explicit in time finite difference characteristic-wise WENO method in a uniform grid following Refs. [18, 34]. Thus, typical wave speeds and vectors, eigenvalues and eigenvectors of the purely hyperbolic part, are correctly resolved.

### III. RESULTS

We have applied the traditional molecular dynamics (MD) approach to compare the results from the two different hydrodynamic models, corresponding to the JR and LG sets of kinetic coefficients. In all simulations, the frequency of the piston motion is  $f = 3.75$  Hz and the amplitude is  $A = 5.6$  particle diameters. The system size is tuned to fit three pattern wavelengths in the (horizontal)  $x$ -direction ( $125\sigma$ ), which is periodic. In the (vertical)  $y$ -direction, the hydrodynamic simulations are constrained into a box of finite height of 60 diameters, whereas the MD system is not limited (particles reach the height of 60 diameters very rarely). The coefficient of restitution is  $\alpha = 0.8$  and disks are of unit mass.

The top and bottom walls in both hydrodynamic simulations are adiabatic and impenetrable. More precisely, the normal velocity is zero at the walls, the energy flux is zero, and the tangential velocity remains unchanged. The simulation is carried over in the comoving frame of the wall, and thus the force per unit mass of the simulated system is  $\vec{F} = -g(1 + A \sin(2\pi ft))\vec{j}$ , with  $\vec{j} = (0, 1)$ .

We refer the reader to Ref. [7] regarding the details of the averaging procedure applied to the MD sequence, here consisting of 1,000 cycles, which leads to the averaged MD hydrodynamic fields for the density (packing fraction), linear momentum and thermal energy. From the latter, the temperature field is also obtained. These are compared to the corresponding ones generated by the two hydrodynamic simulations.

We disregard the transient originating from the initial condition until the pattern of the Faraday instability has fully developed and no changes are observed from period to period. After this transient time, which takes about 50 periods of forcing, the system reveals a subharmonic periodic dynamics where the period is twice the period of the forcing  $f^{-1}$ . In this regime, we fix the reference time,  $t = 0$  and consider the evolution of the profiles of packing fraction, Fig. 3, scaled thermal energy, Fig. 4, scaled granular temperature, Fig. 5 and scaled kinetic energy, Fig. 9 using Eq. (29). The subfigures (a-h) correspond to the times  $t = 0; 1/4f^{-1}; 2/4f^{-1}; \dots; 7/4f^{-1}$ . The corresponding position of the piston is  $y = -A \sin 2\pi ft$ . The profiles shown in Figs. 3-5 are taken at a representative location along the abscissa, where the amplitude of the Faraday pattern is developed. The evolution of these profiles over the period of excitation is also presented as supplementary online material [35], showing the profiles at many more intermediate times.

#### A. Density

First of all we are going to discuss the behavior of the packing fraction, Fig. 3. Since the packing fraction is proportional to the number density  $\phi = \pi\sigma^2 n/4$ , then we will use both terms indistinctly. As in subsequent figures, the abscissa represents the height, in diameters.

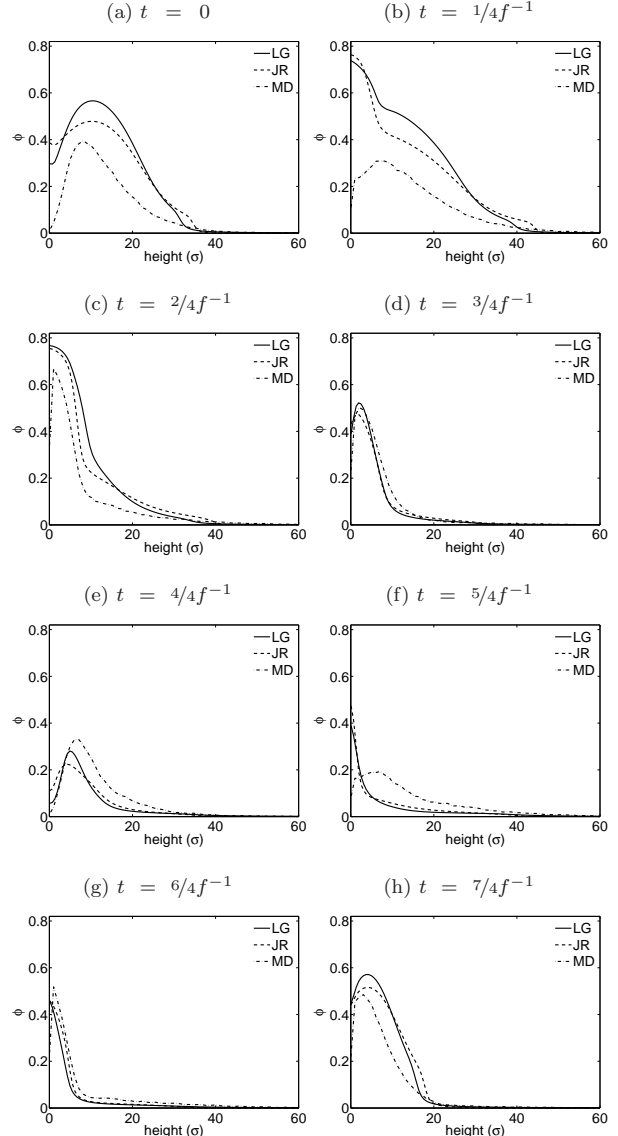


FIG. 3: The profiles of the packing fraction ( $\phi$ ) as a function of height (in units of  $\sigma$ ) at selected times over two oscillation periods. For time evolution of the profiles see [35].

On the ordinate we show here the packing fraction. The evolution is shown from left to right, and then from top to bottom. Note that the integral of each curve is not the same for the HD and the MD simulations since it corresponds just to a vertical cut at a position where the maximum height of the pattern is achieved. Total conservation of mass is maintained in all simulations with high accuracy, see [7] for more details.

At time  $t = 0$ , Fig. 3(a), the piston is going down through the equilibrium position. The height of the ma-

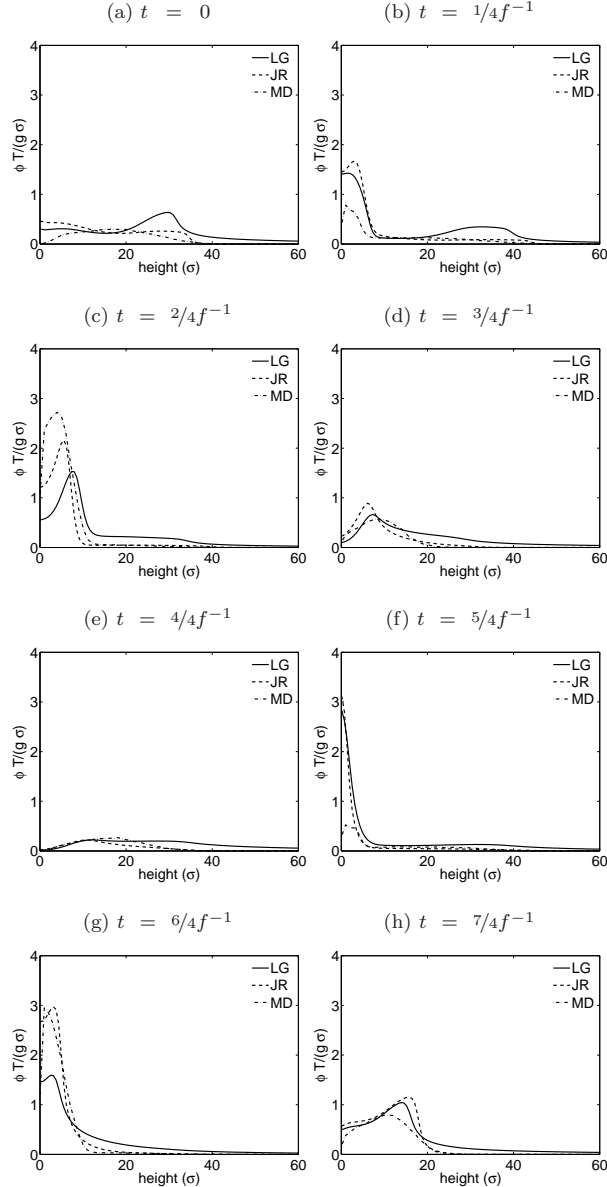


FIG. 4: Scaled internal energy ( $\phi T / (g\sigma)$ ) as a function of height (in units of  $\sigma$ ) at selected times over two oscillation periods. For time evolution of the profiles see [35].

material at this location has already grown to a maximum, formed at the end of the previous cycle (g, h). Shortly after this time the granular layer experiences the impact against the bottom wall and the propagation of a shock wave. Between (a) and (c), we see the dissolution of the peak. We observe that the LG system is denser than the JR at a distance of 10 diameters from the plate. Just instants following frame (c), the layer becomes flat—so does after frame (g), and the material floods to neigh-

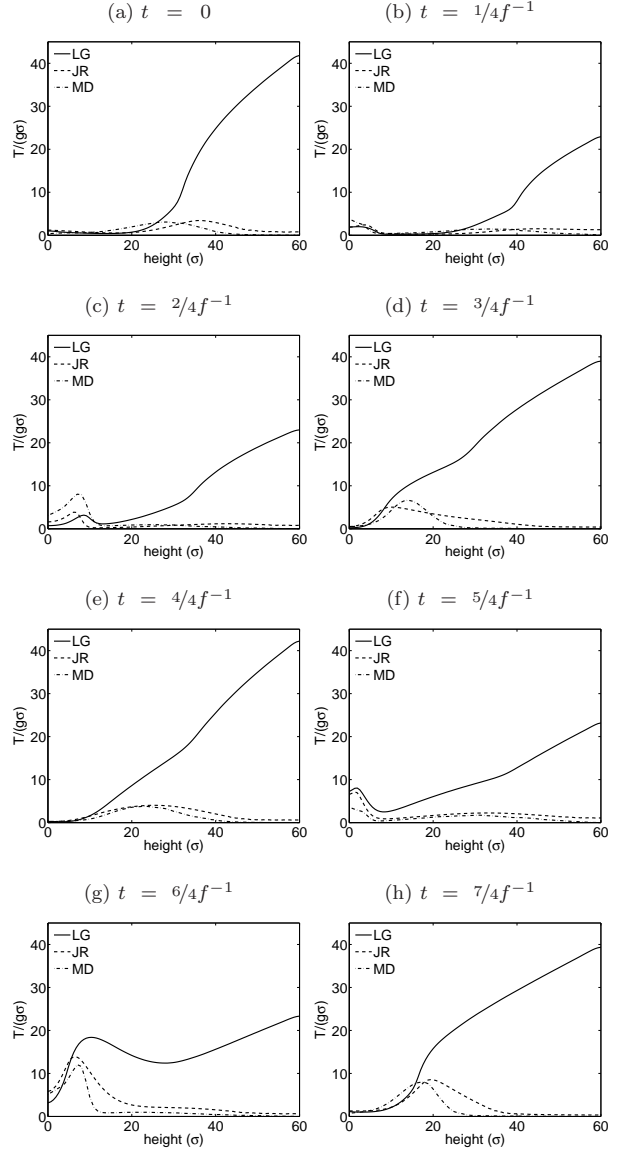


FIG. 5: Profiles of the temperature ( $T / (g\sigma)$ ) as a function of height (in units of  $\sigma$ ) at selected times over two oscillation periods for the MD system and the JR and LG solutions. For time evolution of the profiles see [35].

boring positions to create peaks where valleys previously existed. Shortly after (d), another impact with the plate takes place. From frame (d) to frame (g), we see the evolution of the density at a valley.

The MD sequence reveals that the maximum density 0.69 in packing fraction is smaller than in both hydrodynamic simulations, reaching the value 0.78. This can be due to the irregularity of the MD pattern due to the elasticity of the system at  $\alpha = 0.80$ , which makes the location of any of the peaks of the MD sequence somewhat

uncertain. We recall that the granular Navier-Stokes solver does not contain fluctuational –mesoscopic– contributions, while the local noise is enhanced by increasing the coefficient of restitution. That is why one needs a factor of 20 times more cycles to obtain smooth fields, as compared with the results at  $\epsilon = 0.75$ , obtained in our previous study [7]. There the regularity was much more pronounced, and a much better agreement was achieved.

While the LG and JR profiles do not differ greatly, there are some differences: the LG density is higher at the core of peaks and valleys, as compared to the JR system at equivalent times. Correspondingly, the packing fraction at the bottom plate is smaller in the LG simulation, and so is the minimum density (0.054 vs. the value of 0.112 obtained in the JR simulation). However, the minimum density in the averaged MD profile is still smaller: 0.004. Also, the impact with the plate occurs later as compared with both hydrodynamic simulations, the delay being about  $0.16f^{-1}$ . Therefore we may argue that in general the LG model for the kinetic coefficients does not greatly improve the density profile obtained with the JR model to match the MD results. A direct comparison of the time evolution of densities and velocity fields in full spacial resolution can be found in the supplementary material [35].

A zoom of the region of the MD system close to the plate during the airborne phase will show a few particles stuck to the base of the peaks and empty areas with no particles at all below the valleys (Fig. 6). As a consequence, the impact of the wall against the material happens at  $t = 0.16f^{-1}$  (instead of  $t = 0$ ). We want to remark that this piece of the system is not in the hydrodynamic regime at this moment, but in the Knudsen regime, and there is little hope that any hydrodynamic model can reproduce this feature in full detail. However the LG model improves the dynamics of the gap formed as compared with the JR model in the sense that the minimum density at the bottom plate is reduced. On the other hand, the density gradients are higher in the LG model, a feature which is not observed in the MD profiles, which are smoother. The differences are basically due to the presence of the coefficient  $\mu_{LG}$  (Eq. (19) of the LG model), which is absent ( $\mu_{JR} = 0$ ) in the JR theory.

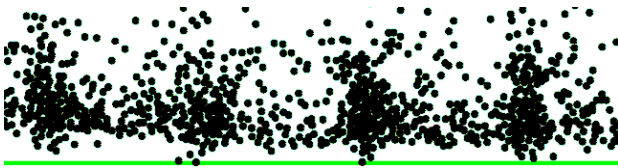


FIG. 6: A snapshot of the MD simulation at the maximum opening of the gap ( $t \approx 0.12 f^{-1}$ ), showing the material stuck at the bottom, between the peaks and the plate, whereas there is a completely empty space below the valleys.

## B. Temperature and internal energy

In Figure 4 we plot the scaled internal energy,  $\phi T/(\sigma g)$ , where  $g$  denotes the gravity acceleration. Here we see the evolution of the shock wave travelling across the granular layer. We can observe that the energy is smaller everywhere in the LG system, except at intermediate and large heights. Remarkably, the energy of the LG shock wave is lower than the JR after an impact with the wall, however the remnants persist for long at larger heights. The MD profile indicates a higher energy at the bottom after an impact (c), as compared with both LG and JR results, but specially with the latter. The LG shock wave is very much damped. It also shows that the impact with the bottom wall occurs effectively later, as pointed out when discussing the density profiles. In addition, the MD profile shows that the energy vanishes quicker than in the LG solution. Let us examine then the temperature field.

The most striking difference between the LG and JR solutions is the temperature field, Fig. 5. At large heights, the LG temperature is one order of magnitude larger than the JR. Moreover, the LG temperature gradient is positive at middle heights (it starts to grow) whereas there the JR, like the MD temperature gradient, is negative once the shock wave is dissipated. It is clear that the term  $\mu \nabla n$  helps to sustain large temperature gradients in the system, transferring heat from the dense to the dilute regions at the top wall. This term is the genuine contribution of the higher order expansions to the kinetic coefficients, although we find no hint in the obtained MD profile that the temperature gradient should be positive instead of negative when ascending from the dense to the dilute region.

As the LG temperature is higher than the JR temperature at the top, the LG solution is more diffusive. Figure 7 shows the vertical component of the heat flux as a function of height, where this effect is shown: note the enhanced heat transport at intermediate heights, as compared with the JR solution. Unlike the JR case, the LG heat flux consists of two terms, the one coming from the temperature gradient, and the one associated, through the coefficient  $\mu$ , to the density gradient. An analysis of the data reveals that both terms have generally opposite signs. The role of the latter contribution is to transfer heat from the dense towards the dilute regions at the top, while the former brings energy into the granulate, from the high temperature regions at the top. Both terms are relevant and contribute in the same order of magnitude. So, the heat transfer dynamics is quite different in the LG and the JR models, not only at the top but also at the bottom plate when the impacts occur, in such a way that gives rise to entirely different solutions for the temperature field.

In general, the LG system is less diffusive very close to the plate and more at intermediate heights and at the top, as compared with the JR system. The viscosities and the cooling term (see Fig. 8) also follow this pattern. The analysis of the results allows us to conclude that

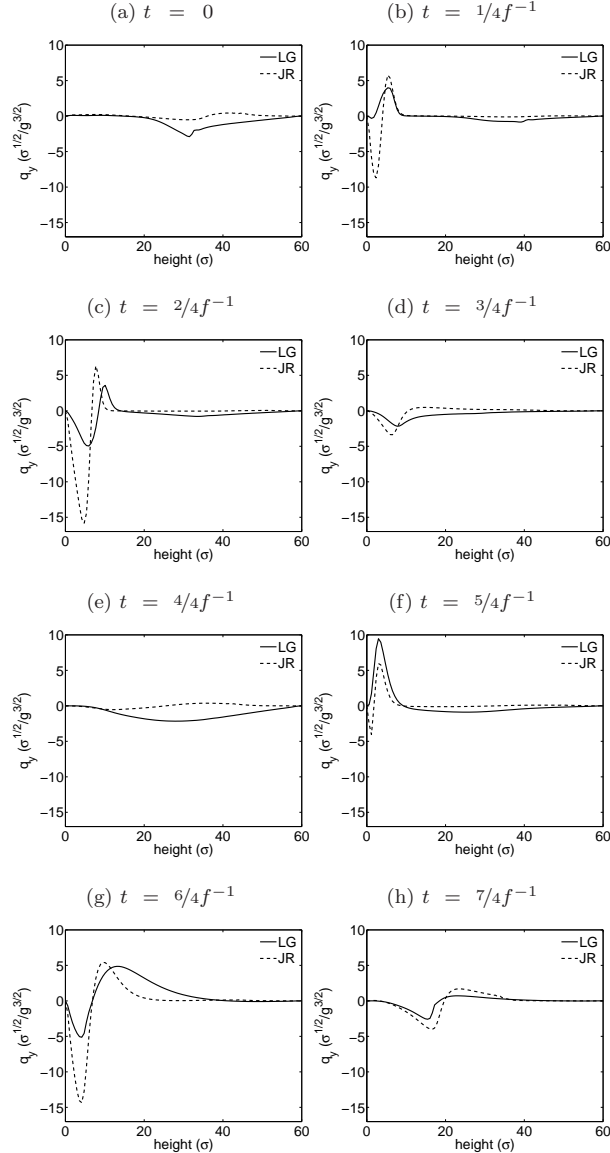


FIG. 7: Vertical component of the (reduced) heat flux as a function of height (in units of  $\sigma$ ) at selected times over two oscillation periods, for the JR and LG simulations. For time evolution of the profiles see [35].

in the JR system, most of the energy is dissipated very close to the plate, whereas much less is diffused; in the LG, comparatively, there is less dissipation at the plate and more diffusion.

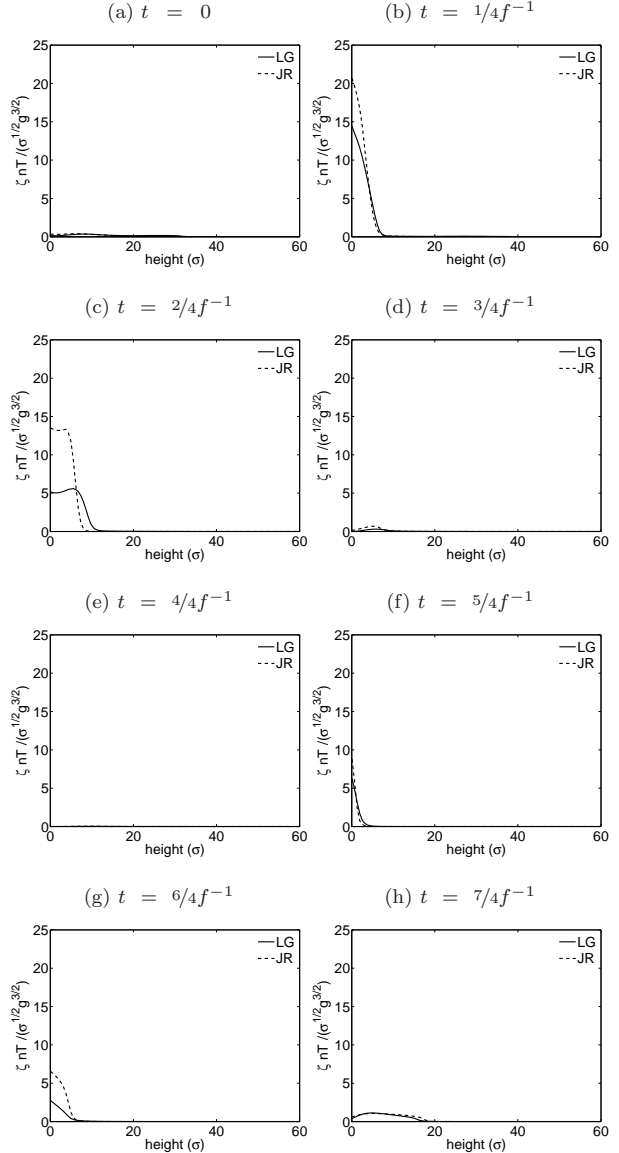


FIG. 8: The profiles of the cooling term  $\zeta n T$  as a function of height (in units of  $\sigma$ ), at selected times over two oscillation periods, for the JR and LG simulations. For time evolution of the profiles see [35].

### C. Kinetic energy and Mach number

Figure 9 shows the scaled kinetic energy profiles. An examination of the entire sequence shows that the maximum of the kinetic energy is achieved at  $t = 0.38 f^{-1}$  in the LG simulation, at  $t = 0.42 f^{-1}$  in the JR and at  $t = 0.54 f^{-1}$  in the MD. The LG peak is the highest, more than 4 times bigger than the MD, and about 50% bigger than the JR. This shows that the LG solution for

the velocity field is also quantitatively different from the JR, a consequence of the inelasticity contributing to the viscosities. Leaving aside the mismatch at the maximum, the JR and LG solutions go close to each other, and differently from the MD profile, due to the delayed landing of the granular layer in the MD simulation. In any case the comparison of the kinetic energy profiles reinforces the quite unexpected result that the LG solution is not closer to the MD, but even further away, than the JR.

Since the LG temperature is about one order of magnitude higher than JR in the dilute region, the Mach number is also smaller. In Fig. 10 we can see how the differences are very relevant during the stages (c)-(d), when the layer has achieved its maximal extension, and where the JR Mach number is about twice that of the LG. This is another fact showing that the LG system is more diffusive than the JR.

The MD curve for the Mach number has been produced using the averaged density and temperature fields into Eq. (30) for the soundspeed, supplied with the equation of state (13).

Unlike JR and LG theory, the second MD peak in the Mach number is higher than the first one. Anyway LG predicts better the behavior of the Mach number than JR. The values of the Mach number have been computed at the heights shown by the red curves in Fig. 10. They correspond to the first point, going from the dense to the dilute phase, where the packing fraction is 0.1. There we also find discrepancies when comparing the MD results with those of JR and LG simulations. This is a consequence of the discrepancies in the density field discussed above.

#### IV. CONCLUSIONS

We have compared the Jenkins-Richman and the Lutsko-Garzó models for the kinetic coefficients of two dimensional granular gases in a highly nonlinear, far-from-equilibrium problem such as the periodic impact of a horizontal piston which gives rise to the characteristic pattern formation of the Faraday instability. After comparing both theories with coarse-grained MD results, we can conclude on the following relevant aspects.

First, we conclude that the latest knowledge available regarding the kinetic coefficients at the Navier-Stokes level of description is not capable of reducing the discrepancy between discrete particle simulations and hydrodynamic simulations of moderately dense, inelastic gases.

This discrepancy generally increases in the case of the LG theory, making the less appropriate Jenkins-Richman a better choice when it comes to describe the temperature field and the shock wave propagation. This fact refers directly to the modeling of the heat flux as the major source of mismatch.

The coefficient  $\mu$ , characteristic of inelastic gases and thus vanishing in the JR theory, constitutes the significant contribution to an enhanced heat transfer mecha-

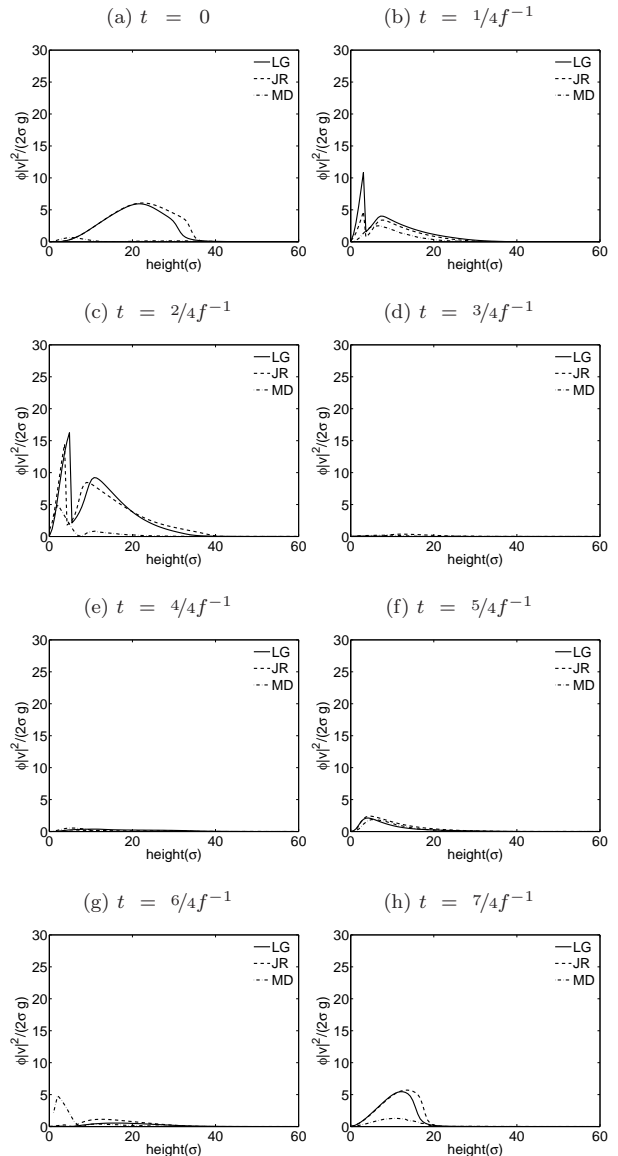


FIG. 9: The scaled kinetic energy profiles as a function of height (in units of  $\sigma$ ), at selected times over two oscillation periods for the MD, JR and LG systems. For time evolution of the profiles see [35].

nism which leads to a high temperature solution in the dilute region, which is not supported by the particle simulations. In fact, if one makes  $\mu = 0$  while keeping the rest of the LG coefficients in the Navier-Stokes equations, a globally better agreement with MD is achieved as compared with JR (result which has not been shown here).

The next level of description, beyond Navier-Stokes, might prove a better approximation to problems like this one, where the first order in the gradients expansion looks insufficient. However it is rather surprising that the coef-

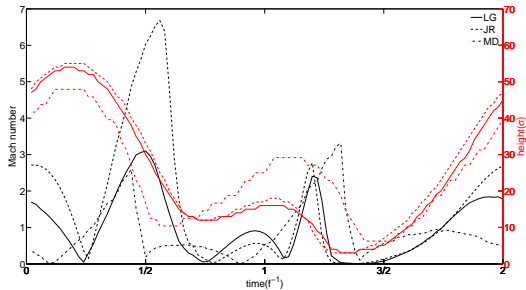


FIG. 10: (color online) Mach number for MD system and JR and LG theories as a function of time, along two periods ( $f^{-1}$ ) of oscillation of the plate. The red curves indicate the variable height (in diameters) which corresponds to the Mach number shown. These heights are found as the first point in vertical direction from the plate where the packing fraction is 0.1.

ficients for the quasielastic gas work better than the more appropriate LG theory in the Navier-Stokes description. Although the entire domain is showing the effects of an altered heat transfer, this is especially true in the dilute region at the top of the system. It is interesting to note that, for a dilute gas, which is the region of larger discrepancies, the coefficient  $\mu$  is very different from zero (Fig. 1).

On the other hand, it has been found that for the simple shear granular flow, the non-Newtonian viscosity to be plugged into the Navier-Stokes equations is better modeled by the elastic than the inelastic theory [30]; here we face a similar situation with respect to the heat flux terms, diffusion mechanism which is governing the

dynamics in our problem.

These discrepancies do not imply that the LG theory is deficient in any respect. Rather differently, they show the limits of the Navier-Stokes description applied to complex granular flow. Indeed, research on other problems has shown its applicability —see for example [36], where MD results of the critical length for cluster formation in the homogeneous cooling state are successfully compared with the predictions from linear stability analysis [37] performed on the basis of the LG kinetic coefficients.

As a global conclusion, the linear theory has shown limitations when exploring the highly nonlinear problem of the granular Faraday instability. In spite of that, both LG and JR models work quite well, although here —as in some other cases, the JR elastic theory is preferable to the more sophisticated LG development.

#### ACKNOWLEDGMENTS

LA and JAC were partially supported by the project MTM2011-27739-C04-02 DGI (Spain) and 2009-SGR-345 from AGAUR-Generalitat de Catalunya. LA, JAC, and CS acknowledge support of the project Ingenio Mathematica FUT-C4-0175. CS and VG appreciate funding from the projects DPI2010-17212 (CS) and FIS2010-16587 (VG) of the Spanish Ministry of Science and Innovation. The latter project (FIS2010-16587) is partially financed by FEDER funds and by the Junta de Extremadura (Spain) through Grant No. GR10158. LA and TP were supported by Deutsche Forschungsgemeinschaft through the Cluster of Excellence *Engineering of Advanced Materials*. JAC is on leave from Department of Mathematics, Imperial College London, London SW7 2AZ, UK.

- 
- [1] J. Jenkins and M. W. Richman, *Arch. Rational Mech. Anal.*, **87**, 355 (1985).
  - [2] J. Jenkins and M. W. Richman, *Phys. Fluids*, **28**, 3485 (1985).
  - [3] C. Bizon, M. D. Shattuck, J. B. Swift, and H. L. Swinney, *Phys. Rev. E*, **60**.
  - [4] E. C. Rericha, C. Bizon, M. D. Shattuck, and H. L. Swinney, *Phys. Rev. Lett.*, **88**.
  - [5] J. Bougie, S. J. Moon, J. B. Swift, and H. L. Swinney, *Phys. Rev. E*, **66** ().
  - [6] J. Bougie, J. Kreft, J. B. Swift, and H. L. Swinney, *Phys. Rev. E*, **71** ().
  - [7] J. A. Carrillo, T. Pöschel, and C. Salueña, *J. Fluid Mech.*, **597**.
  - [8] J. Bougie, *Phys. Rev. E*, **81**.
  - [9] J. Bougie and K. Duckert, *Phys. Rev. E*, **83**.
  - [10] F. Melo, P. Umbanhowar, and H. L. Swinney, *Phys. Rev. Lett.*, **72** ().
  - [11] F. Melo, P. B. Umbanhowar, and H. L. Swinney, *Phys. Rev. Lett.*, **75** ().
  - [12] S. A. Hill and G. F. Mazenko, *Phys. Rev. E*, **67**, 061302 (2003).
  - [13] N. V. Brilliantov, C. Salueña, T. Schwager, and T. Pöschel, *Phys. Rev. Lett.*, **93**, 134301 (2004).
  - [14] B. Meerson, T. Pöschel, and Y. Bromberg, *Phys. Rev. Lett.*, **91** ().
  - [15] B. Meerson, T. Pöschel, P. V. Sasorov, and T. Schwager, *Phys. Rev. E*, **69** ().
  - [16] P. Eshuis, D. van der Meer, M. Alam, H. J. van Gerner, K. van der Weele, and D. Lohse, *Phys. Rev. Lett.*, **104**.
  - [17] M. Faraday, *Phil. Trans. R. Soc. Lond.*, **121**, 299 (1831).
  - [18] C.-W. Shu, in *Advanced Numerical Approximation of Nonlinear Hyperbolic Equations*, Lecture Notes in Mathematics, Vol. 1697, edited by C. Cockburn, B. amd Johnson, C.-W. Shu, and E. Tadmor (Springer, Berlin, 1998) p. 325.
  - [19] J. F. Lutsko, *Phys. Rev. E*, **72**.
  - [20] V. Garzó and J. W. Dufty, *Phys. Rev. E*, **59**.
  - [21] V. Garzó, unpublished notes (2011).
  - [22] A. Goldshtein and M. Shapiro, *J. Fluid Mech.*, **282**, 75 (1995).
  - [23] J. J. Brey, J. W. Dufty, and A. Santos, *J. Stat. Phys.*,

- 87**, 1051 (1997), ISSN 0022-4715.
- [24] N. Brilliantov and T. Pöschel, *Kinetic Theory of Granular Gases* (Oxford University Press, 2004).
- [25] H. Grad, *Comm. Pure Appl. Math.*, **2**, 331 (1949), ISSN 0010-3640.
- [26] D. M. Gass, *J. Chem. Phys.*, **54**, 1898 (1970).
- [27] S. Torquato, *Phys. Rev. E*, **51**.
- [28] S. Chapman and T. G. Cowling, *The mathematical theory of non-uniform gases. An account of the kinetic theory of viscosity, thermal conduction and diffusion in gases*, Third edition, prepared in co-operation with D. Burnett (Cambridge University Press, London, 1970) pp. xxiv+423.
- [29] I. Goldhirsch, *Annu. Rev. Fluid Mech.*, **35**, 267 (2003).
- [30] A. Santos, V. Garzó, and J. W. Dufty, *Phys. Rev. E*, **69**.
- [31] J. J. Brey and M. J. Ruiz-Montero, *Phys. Rev. E*, **70**.
- [32] J. J. Brey, M. J. Ruiz-Montero, P. Maynar, and I. García de Soria, *J. Phys.: Condens. Matter*, **17**, S2489 (2005).
- [33] V. Garzó, A. Santos, and J. M. Montanero, *Physica A*, 94.
- [34] G. Jiang and C.-W. Shu, *J. Comput. Phys.*, **126**, 202 (1996).
- [35] supplementary online material:  
<https://mat.uab.es/~lalmazan>.
- [36] P. P. Mitrano, S. R. Dahl, C. D. J., M. S. Pacella, and C. M. Hrenya, *Phys. Fluids*, **23**.
- [37] V. Garzó, *Phys. Rev. E*, **72**.